International Journal of Innovation in Mechanical Engineering and Advanced Materials
Homepage: publikasi.mercubuana.ac.id/index.php/ijimeam
Vol. 8 (No. 3), 2026, Art. No. 40219, pp. 173-190
DOI: 10.22441/ijimeam.v8i3.40219

Article

Ambient-Temperature Sensitivity of Operating-Data Fouling-Resistance Indicators for an Air-Cooled Condenser in a Binary Geothermal Power Plant

Richard Alexander, Agus Setyawan *, and Udi Harmoko

Master of Energy Program, School of Postgraduate Studies, Universitas Diponegoro, Tembalang, Semarang 50275, Indonesia
*Corresponding Author: agussetyawan@fisika.fsm.undip.ac.id (AS)

Abstract

Air-cooled condensers (ACCs) reject heat directly to the atmosphere, so operating-data fouling indicators are read against a heat sink that moves continuously. This study quantifies how much of the calculated fouling resistance of an ACC serving a 41.75 MW binary geothermal unit is generated by ambient-temperature variation alone, with the physical surface condition held unchanged, and establishes how that component depends on whether cooling-air flow is measured or inferred. A zone-resolved thermal model was built from bundle geometry, plant working-fluid states and a measured fan air velocity of 6.02 m s^{-1}, with n-pentane and air properties taken from CoolProp. The indicator was evaluated over the observed ambient range of 18.63 to 29.56 °C under three routes that differ only in which air-side quantity is measured. Ambient variation alone moved the indicator by 2.22 × 10^{-2} m^2 K W^{-1} across the mean daily range, which exceeded its own mean value by a factor of 3.3 and reversed its sign at 24.5 °C although the surface condition did not change. The negative values carry no physical meaning, because a deposit cannot reduce thermal resistance. The sign of the reported trend followed the air-side assumption rather than the equipment, and four clean-condition treatments shifted the level of the indicator without altering its ambient slope, which stayed negative in 100 % of 2,000 Monte Carlo samples. The calculated resistance therefore measures the ambient sensitivity of the method and not the fouling state of the bundle. Matched-ambient comparison bands, a plant-specific clean baseline and independent air-side indicators are required before it can support a cleaning or maintenance decision.

Article Info:
Received: 14 September 2026
Revised: 19 October 2026
Accepted: 26 October 2026
Available online: 23 November 2026

Keywords:
air-cooled condenser; fouling resistance; ambient temperature; overall heat-transfer coefficient; binary geothermal power plant; condition monitoring

© 2026 The Authors. Published by Universitas Mercu Buana (Indonesia). This is an open-access article, distributed under *CC BY-SA* License.

1. Introduction

Binary geothermal plants in water-constrained locations reject the whole cycle heat load to ambient air, so the condenser terminal temperature is set by weather rather than by a cooling tower approach. That penalty is measurable at plant scale. Kahraman et al. report that the net output of a 21 MW air-cooled binary unit falls by 6.8 MW as ambient temperature rises through 30 K, a loss of roughly 32 % of nameplate capacity driven entirely by the heat sink [1]. Astolfi et al. show the same mechanism in cycle optimisation. For medium-enthalpy resources the condensing pressure imposed by the air-cooled condenser (ACC) is the single parameter that most constrains achievable second-law efficiency [2]. At the unit examined here the observed ambient range spans 10.93 K within a single 59-day record and 6.57 K within an average day, so the heat sink moves across a large part of its annual range every 24 hours. The cycle of the unit examined here is shown in Figure 1. The ACC closes the working-fluid loop, so it is the only component whose cold terminal is set outside the plant, and every ambient movement reported below enters the cycle at that point.

Against this moving background, operators must still decide when the condenser needs cleaning. Deposition on the finned bundle adds an air-side thermal resistance that raises condensing pressure and reduces turbine output, and field and laboratory studies confirm that

How to cite:

R. Alexander, A. Setyawan and U. Harmoko, "Ambient-temperature sensitivity of operating-data fouling-resistance indicators for an air-cooled condenser in a binary geothermal power plant," *Int. J. Innov. Mech. Eng. Adv. Mater.*, vol. 8, no. 3, pp. 173-190, 2026.

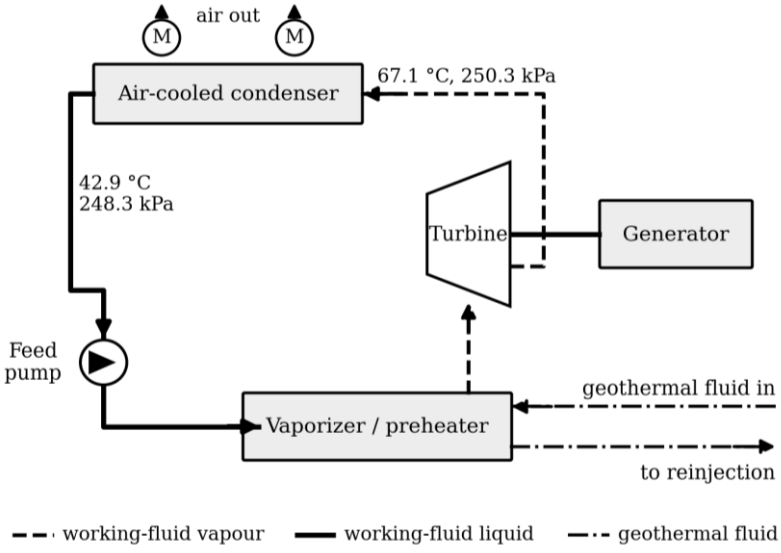


Figure 1. Organic Rankine cycle configuration of the investigated binary unit, with the air-cooled condenser closing the working-fluid loop.

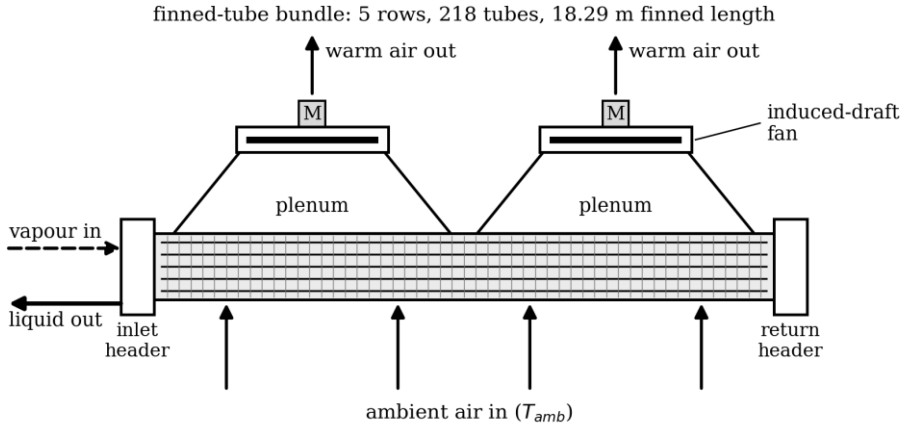


Figure 2. Induced-draft finned-tube ACC bundle with working fluid inside the tubes and ambient air drawn upward across the finned bank by the fans.

particulate deposits produce measurable reductions in the overall heat-transfer coefficient of finned-tube air coolers [8], [9]. Direct inspection of the fin surfaces requires an outage, which no operator will schedule on suspicion alone. Condition is therefore inferred from operating data by comparing the overall coefficient obtained from measured duty and temperatures against a clean-condition coefficient assembled from correlations, with the difference of reciprocals reported as a fouling resistance [10], [11]. Figure 2 shows the configuration of the exchanger on which this inference is performed.

This inference is reliable only when every quantity feeding it is measured. In an ACC it is not. The air-side film coefficient governs the largest single resistance in the network, yet it is never measured directly. It is estimated from a correlation that requires air flow, which on most plants is itself not logged. Ambient temperature enters the calculation twice and in opposite directions. It fixes the cold terminal of the log-mean temperature difference that produces the operating coefficient, and it sets the air properties that produce the clean-condition coefficient. When the two coefficients respond to ambient temperature at different rates, their difference of reciprocals moves even though the surface has not changed. The indicator is then reporting the weather.

Three bodies of work bear on this problem, and none of them closes it. The first establishes the ambient sensitivity of air-cooled binary plants but treats it as a cycle-performance

question, reporting power output or exergy efficiency against ambient temperature rather than asking what the same variation does to a condition indicator [1], [2], [3], [4]. The second characterises air-side fouling of finned bundles experimentally, establishing deposition rates and the associated loss of overall coefficient, but does so under controlled laboratory air conditions in which ambient temperature is held constant precisely so that the fouling signal can be isolated [7], [8], [9]. The third addresses fouling monitoring from operating data and has already identified one structural failure mode of the overall-coefficient method. Patil et al. show that when a control loop holds duty constant, the indicator stops responding to real deposition because the controller absorbs the degradation [12]. That result matters here because it establishes the principle that the monitoring method inherits the dynamics of whatever holds the exchanger at its operating point. An ACC has no controller holding duty constant. It has a heat sink that moves. The analogous distortion has not been quantified.

The quantitative comparison between those studies and the present problem turns on the conditions under which each fouling metric is obtained. Studies of fouling mitigation on heat exchanger surfaces report their effect as a change in fouling resistance or in the overall coefficient measured with inlet temperatures and flow rates held fixed [20], [21], [22], [23], [24], [25], and the experimental air-side studies of finned bundles impose the same control [7], [8], [9]. Holding the thermal boundary fixed is what allows a deposition signal to be separated from the operating condition that produced it. In the ACC examined here the ambient-generated component of the same indicator reached 2.22×10^{-2} m^2 K W^{-1} over an average day, which is equivalent to a 25.0 % reduction in the clean overall heat-transfer coefficient of 15.0 W m^{-2} K^{-1}. This artefact is therefore of the same order as the deposition signals those studies set out to resolve, and it appears on a condenser whose surface condition has not changed.

The gap is therefore a specific missing combination rather than a general shortage of studies. The propagation of ambient-temperature variation through a conventional operating-data fouling-resistance calculation for an air-cooled condenser, evaluated for its dependence both on the clean-condition heat-transfer model and on whether cooling-air flow is measured or inferred from an assumed air outlet temperature, has not been established for

Table 1. ACC geometry, derived areas and material parameters.

Parameter	Value	Unit
Bundle width × length	2,646 × 18,980	mm
Tube rows / passes	5 / 1	–
Number of tubes	218	–
Tube outside diameter, D_o	25.4	mm
Tube inside diameter (BWG 16), D_i	22.098	mm
Finned tube length, L	18,292	mm
Layout / transverse pitch, P_T	60° triangular / 58.7	mm
Fin density, n_f	10	fins in^{-1}
Fin outside diameter, D_f	57	mm
Fin height / thickness, b/τ	15.8 / 0.3	mm
Tube and fin material	S235JR	–
Wall thermal conductivity, k_w	40	W m^{-1} K^{-1}
Bare tube outside area, A_o	318.2	m^2
Prime (unfinned) area, A_{prime}	280.6	m^2
Fin area, A_{fin}	6,505.6	m^2
Total finned outside area, A_{tot}	6,786.2	m^2
Tube inside area, A_i	276.8	m^2
Frontal area, A_{fr}	48.40	m^2
Free-flow ratio, σ	0.5037	–
Minimum free-flow area, A_{min}	24.38	m^2
Air-side hydraulic diameter, D_h	3.65	mm
Bundles per unit	20	–

a binary geothermal ACC. Its second half carries the operational consequence, because it determines whether the distortion can be removed by better instrumentation or is inherent to the formulation.

This study quantifies the ambient-temperature-generated component of the calculated fouling resistance of the ACC serving a 41.75 MW binary geothermal unit. Ambient temperature is the imposed variable, swept over the 18.63 to 29.56 °C range observed in a 59-day plant record. Measured inputs are the working-fluid inlet, condensing and outlet states, the bundle duty, the bundle geometry and a single fan velocity of 6.02 m s^{-1} over a fan area of 18.7 m^2. Calculated parameters are the clean-condition and operating overall heat-transfer coefficients and the fouling resistance formed from their reciprocals. The reference condition is the clean-condition coefficient assembled from correlations at each ambient temperature, against which the operating coefficient is compared. Magnitude, sign and robustness of the resulting ambient dependence are the outcomes evaluated, together with whether that dependence survives changes in the clean-condition model, parameter perturbation and the choice of which air-side quantity is measured.

2. Methods

2.1. Plant, dataset, and condenser geometry

This study examines a binary geothermal power plant in Pahae Julu and Pahae Jae, North Tapanuli, North Sumatra, Indonesia, using n-pentane as the working fluid in a closed organic Rankine cycle. Geothermal brine vaporises the working fluid, which expands through the organic turbine before entering an induced-draft finned-tube ACC. Desuperheating,

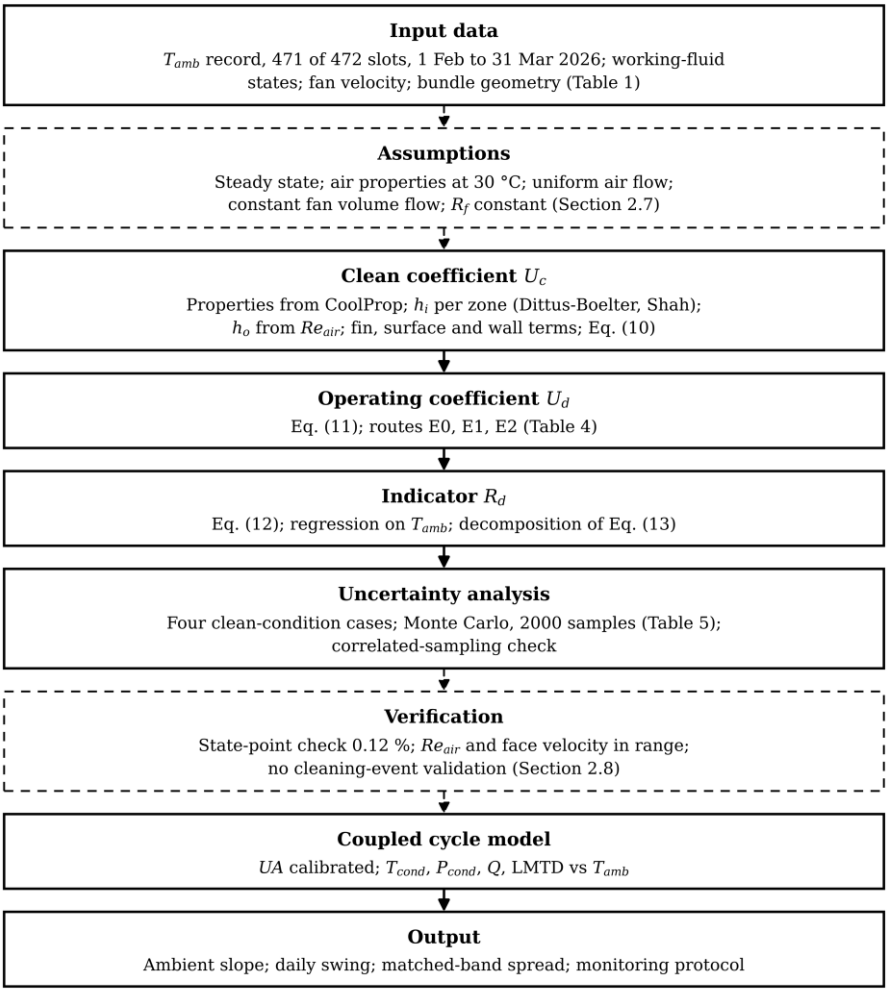


Figure 3. Calculation workflow from plant inputs to the reported ambient sensitivity of the fouling indicator, with the assumptions, the verification status and the uncertainty analysis shown as explicit stages.

condensation and subcooling all take place in the condenser before the condensate is returned by the feed pump. Each unit carries 20 identical bundles. The analysis was performed on one bundle and reported per bundle unless stated otherwise.

Table 1 gives the geometry. Every derived area is recomputed from the stated dimensions rather than carried from the design data sheet, so that a reader can reproduce each value. Free-flow ratio, minimum free-flow area and air-side hydraulic diameter are reported because the air-side correlation and Reynolds number depend on them directly.

Observations in the plant record fall at nominal three-hour intervals, eight per day, over the 59 days from 1 February to 31 March 2026, giving 471 usable ambient-temperature values after duplicated columns are collapsed and the one empty slot is removed from the 472-slot grid. The only air-side measurement available is a fan velocity of 6.02 m s^{-1} referred to a fan area of 18.7 m^2 per bay, taken from the fan data sheet. No time-resolved record of fan speed, fan current or air outlet temperature exists for the period, and the consequences of that are addressed in Section 3.7.

Figure 3 sets out the complete calculation sequence, from these inputs to the reported indicator.

2.2. Thermophysical properties and working-fluid states

Thermophysical properties of n-pentane and of air are evaluated with the CoolProp library, which implements the Helmholtz-energy reference equations of state, so that every property used in the model is traceable to a published formulation rather than to a tabulated design value [16]. Working-fluid states are the plant-recorded values listed in Table 2. Air specific heat is treated as constant at the value for dry air at 30 °C and 101.325 kPa, $c_{p,air}$ = 1,006.5 J kg^{-1} K^{-1}. Across the 18.63 to 29.56 °C range swept here the true value varies by less than 0.05 %, so the constant-property treatment introduces an error two orders of magnitude below the effects under investigation.

The 0.12 % agreement between the CoolProp saturation pressure at the recorded condensing temperature and the independently recorded outlet pressure is an internal consistency check on the state points. Recorded temperature and pressure describe the same saturation state to within instrument resolution.

Condenser duty follows from the working-fluid enthalpy change, obtained using Equation (1).

$$Q = \dot{m}\,\Delta h = \dot{m}(h_{in} - h_{out}) \tag{1}$$

where Q is the heat transfer rate (W), ṁ is the working-fluid mass flow rate (kg s^{-1}), and h_{in} and h_{out} are the specific enthalpies at the condenser inlet and outlet (J kg^{-1}) evaluated at the recorded temperature and pressure. An enthalpy form is used in place of a specific-heat form because the working fluid changes phase inside the condenser, so no single specific heat applies across the exchanger.

Table 2. Working-fluid states, duty and zone distribution used in the thermal model.

Quantity	Value	Unit
Condenser inlet (superheated vapour)	67.1 / 250.3	°C / kPa
Condensing temperature, T_{cond}	65.2	°C
Saturation pressure at T_{cond} (CoolProp)	248.6	kPa
Recorded condenser outlet pressure	248.3	kPa
Condenser outlet (subcooled liquid)	42.9 / 248.3	°C / kPa
Specific enthalpy change, Δh	391.0	kJ kg^{-1}
Unit duty, Q_{unit}	41.75	MW
Bundle duty, Q	2.0875	MW
Working-fluid flow per unit	106.78	kg s^{-1}
Working-fluid flow per bundle	5.339	kg s^{-1}
Desuperheating share of duty	0.92	%
Condensation share of duty	85.05	%
Subcooling share of duty	14.03	%

2.3. Air-side model

The air side carries the largest resistance in the network, so the treatment of air flow determines the behaviour of everything downstream. Two physically different treatments are possible with the data available, and the distinction between them is the subject of this study rather than an incidental modelling choice.

In the base case the air mass flow is fixed by the measured fan data and the bundle frontal area, using Equation (2). Fan data give an average velocity of 6.02 m s^{-1} referred to a fan area of 18.7 m^2, so the volumetric flow is 112.57 m^3 s^{-1} per bay and the face velocity at the bundle is 2.33 m s^{-1}, within the 2 to 4 m s^{-1} typical of finned ACC bundles.

$$\dot{m}_{air} = \rho(T_{amb}) A_{fr} V_{face} \tag{2}$$

where $\dot{m}_{air}$ is the cooling-air mass flow rate (kg s^{-1}), ρ is the air density at ambient conditions (kg m^{-3}), A_{fr} is the bundle frontal area (m^2) and V_{face} is the face velocity (m s^{-1}). Because the fans are fixed-pitch and run at constant speed, the volumetric flow is treated as constant and the mass flow varies only through air density, falling 3.6 % across the observed ambient range.

The air outlet temperature then follows from the air-side energy balance, Equation (3), as an output of the model rather than an input to it. This is the structural difference from the conventional treatment, in which the outlet temperature is imposed and the air flow is derived from it. When the outlet temperature is imposed, the air-side duty equals the working-fluid duty by construction and the air side carries no independent information. Detailed models of air-cooled finned-tube condensers that resolve the air-side temperature distribution report the same dependence of the predicted performance on how the air side is closed [26].

$$T_{air,out} = T_{amb} + \frac{Q}{\dot{m}_{air}\, c_{p,air}} \tag{3}$$

where $T_{air,out}$ is the air outlet temperature (°C), T_{amb} is the ambient temperature (°C), Q is the bundle duty (W) and $c_{p,air}$ is the specific heat of air (J kg^{-1} K^{-1}).

Air-side Reynolds number is formed on the maximum velocity between the fins and the finned tube outside diameter, using Equations (4) and (5).

$$V_{max} = \frac{P_T\, V_{face}}{P_T - D_f - 2\, n_f\, b\, \tau} \tag{4}$$

$$Re_{air} = \frac{\dot{m}_{air}\, D_r}{A_{min}\, \mu} \tag{5}$$

where V_{max} is the maximum air velocity between the fins (m s^{-1}), P_T is the transverse tube pitch (m), D_f is the fin outside diameter (m), n_f is the number of fins per unit length (m^{-1}), b is the fin height (m), τ is the fin thickness (m), D_r is the fin root diameter, equal to the tube outside diameter (m), A_{min} is the minimum free-flow area (m^2) and μ is the dynamic viscosity of air (Pa s) evaluated at the mean air temperature.

The air-side film coefficient follows from the staggered finned-bank correlation of the compact-surface treatment of Kays and London, Equation (6) [18], which is applicable over the Reynolds-number range 7.2 × 10^3 to 7.7 × 10^3 encountered here.

$$h_o = 0.38\, Re_{air}^{0.6}\, Pr^{1/3} \left(\frac{A_{tot}}{A_o}\right)^{-0.15} \frac{k}{D_r} \tag{6}$$

where h_o is the air-side heat-transfer coefficient (W m^{-2} K^{-1}), Pr is the Prandtl number of air, A_{tot} is the total finned outside area (m^2), A_o is the bare tube outside area (m^2) and k is the thermal conductivity of air (W m^{-1} K^{-1}). This area ratio accounts for the reduced effectiveness of the extended surface relative to a bare bank.

Because the fins carry 95.9 % of the outside area, the air-side resistance must be corrected for the temperature gradient along the fin. Fin efficiency for an annular fin of uniform thickness is obtained from the equivalent-length approximation, Equation (7), and combined with the prime area into a weighted surface efficiency, Equation (8).

$$\eta_f = \frac{tanh(m\psi)}{m\psi}, \qquad m = \sqrt{\frac{2h_o}{k_w \tau}} \tag{7}$$

$$\eta_w = 1 - \frac{A_{fin}}{A_{tot}}\left(1 - \eta_f\right) \tag{8}$$

where η_f is the fin efficiency, ψ is the corrected fin length including the curvature correction (m), m is the fin parameter (m^{-1}), k_w is the fin thermal conductivity (W m^{-1} K^{-1}), η_w is the weighted surface efficiency, and A_{fin} and A_{tot} are the fin and total outside areas (m^2). The weighted efficiency is what multiplies h_o in the overall coefficient. Using the bare film coefficient instead overstates the air-side conductance by a factor of roughly two for this geometry.

2.4. Tube-side model and clean-condition coefficient

Phase change occurs inside the tubes, and the three zones have film coefficients differing by an order of magnitude, so a single-zone treatment cannot represent the tube side. Each zone is evaluated with its own correlation and the results are combined on a duty-weighted basis, Equation (9), with the weights taken from the enthalpy shares in Table 2.

$$h_i = \left[\sum_j \frac{\phi_j}{h_{i,j}}\right]^{-1} \tag{9}$$

where h_i is the duty-weighted tube-side coefficient (W m^{-2} K^{-1}), φ_j is the fraction of total duty transferred in zone j, and $h_{i,j}$ is the film coefficient of that zone. The weighting is applied to the resistances rather than the coefficients because thermal resistances in series add. Weighting the coefficients directly would overstate the tube-side conductance.

The correlations applied to each zone, with their sources and ranges of validity, are listed in Table 3. Desuperheating and subcooling are single-phase turbulent flows and use the Dittus–Boelter correlation. The condensing zone uses the Shah correlation for film condensation inside horizontal tubes, integrated over vapour quality from 1 to 0.

A clean-condition overall coefficient is then assembled from the tube-side film, wall and finned air-side resistances in series, all referred to the total finned outside area, using Equation (10).

$$\frac{1}{U_c} = \frac{A_{tot}}{A_i}\frac{1}{h_i} + \frac{A_{tot} ln(D_o/D_i)}{2\pi k_w LN} + \frac{1}{\eta_w h_o} \tag{10}$$

where U_c is the clean-condition overall heat-transfer coefficient (W m^{-2} K^{-1}), A_i is the tube inside area (m^2), D_o and D_i are the tube outside and inside diameters (m), L is the finned tube length (m) and N is the number of tubes. Each of the three terms is referred to A_{tot} so that they are additive. An area ratio on the tube-side term and the length–count product in the wall term perform that referral.

2.5. Operating coefficient, the indicator and the three evaluation routes

An operating coefficient is obtained from the bundle duty and the corrected log-mean temperature difference, Equation (11), with the correction factor taken from the cross-flow relations for both fluids unmixed.

Table 3. Heat-transfer correlations, their sources and the conditions at which they are applied.

Term	Correlation	Source	Condition in This Model
Desuperheating, $h_{i,dsh}$	Dittus–Boelter	[10]	$Re = 1.89 \times 10^5$, $Pr = 0.76$
Condensation, $h_{i,cond}$	Shah (1979), quality-averaged	[17]	$Re_{L0} = 1.17 \times 10^4$, $Pr = 0.074$
Subcooling, $h_{i,sub}$	Dittus–Boelter	[10]	$Re = 1.05 \times 10^4$, $Pr = 3.26$
Air side, h_o	Staggered finned bank, Eq. (6)	[18]	$Re_{air} = 7.2 \times 10^3$ to 7.7×10^3
F_{in} efficiency, η_f	Annular fin, equivalent length	[18]	$\eta_f = 0.521$ at mean ambient
LMTD correction, F	Cross-flow, both fluids unmixed	[19]	$F = 0.882$ to 0.928

$$U_d = \frac{Q}{A_{tot}\, F\, LMTD} \tag{11}$$

where U_d is the operating overall heat-transfer coefficient (W m^{-2} K^{-1}), $LMTD$ is the log-mean temperature difference formed from the four terminal temperatures (K) and F is the cross-flow correction factor. This correction factor is retained rather than assumed equal to unity because it falls to 0.882 at the top of the ambient range, and omitting it would itself introduce a 10 % ambient-dependent bias into the operating coefficient.

The indicator examined in this study is the difference of the reciprocals of the two coefficients, Equation (12). It is referred to throughout as the calculated fouling resistance, to keep in view that it is a model output and not a measurement.

$$R_d = \frac{1}{U_d} - \frac{1}{U_c} \tag{12}$$

where R_d is the calculated fouling resistance (m^2 K W^{-1}). Monitoring practice treats R_d as equal to the physical fouling resistance R_f. The decomposition that this study sets against that identification is stated in Equation (13).

$$R_d = R_f + R_{amb} + R_{model} + R_{op} \tag{13}$$

where R_f is the physical fouling resistance, R_{amb} the component generated by ambient variation, R_{model} the component generated by error in the clean-condition estimate, and R_{op} the component generated by other operating conditions (all in m^2 K W^{-1}). This decomposition is conceptual, because the four terms cannot be separated without independent identification of each. The present analysis isolates R_{amb} by holding R_f and R_{op} constant by construction, and exposes R_{model} by varying the clean-condition treatment.

Equation (13) also fixes what the analysis can and cannot establish. Because R_f and R_{op} are held constant by construction across the sweep, any movement of R_d with ambient temperature is R_{amb}, so the result is a property of the calculation method and not a statement about the deposit on the bundle. Ambient correction is required before R_d can support a maintenance decision for the same reason. A cleaning decision compares the present value of the indicator against an earlier value or against a threshold, and unless the two are taken at the same ambient temperature the comparison carries a difference of R_{amb} that has nothing to do with surface condition. Two corrections follow directly from the structure of Equation (13) and are evaluated in Section 3.6. Restricting the comparison to a narrow ambient band bounds R_{amb} to the product of the band width and the measured slope, and referencing the indicator to a plant-specific clean baseline expressed as a function of ambient temperature removes R_{model}, which Section 3.4 shows to be the term that sets the level.

The indicator is then evaluated along three routes that differ only in which air-side quantity is treated as known, as set out in Table 4. Route E0 is the base case, in which air flow comes from the measured velocity and the air outlet temperature is computed. Route E1 reproduces the conventional design-referenced treatment, in which duty and condensing temperature are held at their design values and the air outlet temperature is imposed. Route E2 uses the measured working-fluid states with the air outlet temperature still imposed, which is what a plant monitoring system would compute from a data sheet in the absence of air-flow instrumentation. Comparing the three isolates the contribution of the air-side assumption itself.

Table 4. Evaluation routes, the measured and assumed quantities, and what each route tests.

Route	Air-Side Treatment	Working-Fluid Treatment	What The Route Tests
E0 (base case)	Air flow fixed from the measured fan data, 112.57 m^3 s^{-1} per bay; $T_{air,out}$ computed from Eq. (3)	Recorded states and bundle duty	Ambient response when the air side carries independent information
E1	$T_{air,out}$ imposed at the design value; air flow derived from Eq. (2) rearranged	Duty and Tcond held at design values	The conventional design-referenced calculation
E2	$T_{air,out}$ imposed at the design value; air flow inferred	Recorded states, duty from the coupled model	Plant practice with a data-sheet outlet temperature and no air-flow measurement

2.6. Coupled closed-loop model

Holding condenser duty and condensing temperature fixed while ambient temperature varies is thermodynamically inconsistent for a closed cycle, because the condensing temperature is set by the balance between heat rejection and the available driving force. A coupled model is therefore solved alongside the indicator analysis to establish how far the real operating point moves. The fan volumetric flow is held at the measured value, the exchanger conductance is calibrated at the mean-ambient operating point, and the condensing temperature is found by simultaneous solution of the effectiveness–NTU relation and the working-fluid energy balance, with the saturation pressure following from the converged condensing temperature. Solving returns the condensing temperature, condensing pressure, bundle duty and log-mean temperature difference as functions of ambient temperature.

2.7. Sensitivity, uncertainty and assumptions

Two robustness tests are applied. The first varies the clean-condition treatment across four alternatives, namely the duty-weighted tube-side coefficient of Equation (9), condensation only, single-phase liquid only, and zero tube-side resistance. These four span the range of simplifications an analyst might reasonably adopt. The second is a Monte Carlo perturbation of 2,000 samples, in which the air-side coefficient is perturbed by ±25 %, the tube-side coefficient by ±40 %, the heat-transfer area by ±3 %, the duty by ±2 % and the air velocity by ±15 %, all drawn from independent uniform distributions. The two tests address different questions. The first asks whether the ambient dependence survives a change of model, and the second whether it survives a change of parameter values within that model.

Perturbation ranges were set from the accuracy of the quantity that produces each parameter rather than chosen for convenience, and the basis of each is given in Table 5.

All five parameters were drawn from independent uniform distributions, which requires justification because some of them are physically linked. A uniform distribution is the maximum-entropy choice over a bounded interval when the available information supplies a credible range but no shape within it, and treating bounded parameters as independent explores a larger volume than treating them as correlated. Two of the links are real. The air-side coefficient follows the air velocity through Equation (6), in which h_o varies with Re_{air} raised to the power 0.6, and the tube-side coefficient follows the duty through the working-fluid flow. Repeating the analysis with a Gaussian copula imposing a correlation of 0.7 on each of those two pairs left the ambient slope negative in 100 % of samples and changed its 5th to 95th percentile band by less than 1 %, while widening the percentile band on the mean level by about 7 %. Correlation among the inputs therefore alters the spread of the level and leaves the ambient dependence that this study reports unchanged.

Steady state is assumed at each observation, which is acceptable at three-hour spacing but not for transients. Air properties are treated as constant at a 30 °C reference, justified in Section 2.2. Uniform air distribution across the bundle face is assumed, since no measurement of maldistribution is available. Fan volumetric flow is treated as constant, consistent with fixed-pitch blades at constant speed. Physical fouling is held constant across the sweep by construction, which is what permits R_{amb} to be isolated. The analysis therefore reports the ambient-generated component and makes no claim about the actual deposition state of the bundle.

Table 5. Basis for the parameter ranges used in the Monte Carlo perturbation.

Parameter	Perturbation	Basis for The Range
Air-side coefficient, h_o	±25 %	Scatter of the staggered finned-bank correlation of Equation (6) against compact-surface test data [18]
Tube-side coefficient, h_i	±40 %	Combined scatter of the Dittus–Boelter and Shah correlations over the zone conditions of Table 3 [17], [19]
Heat-transfer area, A_{tot}	±3 %	Fin pitch and fin height manufacturing tolerance applied to the derived areas of Table 1
Bundle duty, Q	±2 %	Working-fluid temperature and pressure instrument resolution propagated through Equation (1)
Air velocity, V_{face}	±15 %	Fan data-sheet tolerance together with the absence of a logged fan-speed record (Section 3.7)

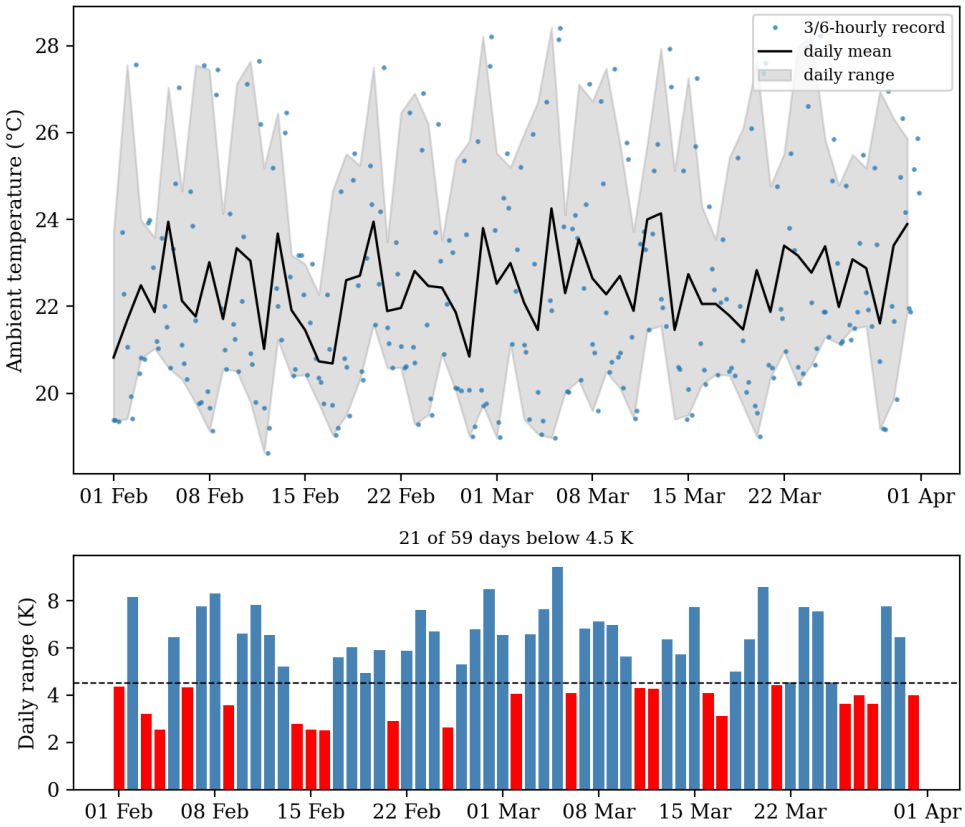


Figure 4. Ambient conditions at the condenser fan inlet, 1 February to 31 March 2026: Observation record with daily mean and daily range (Top); daily range, with the 21 days below 4.5 K shown in red (Bottom).

2.8. Verification checks and validation status

Four verification checks were applied to the model before the ambient sweep was run. The saturation pressure returned by CoolProp at the recorded condensing temperature agreed with the independently recorded outlet pressure to 0.12 %. A face velocity of 2.33 m s^{-1} derived from the fan data fell inside the 2 to 4 m s^{-1} range normal for finned ACC bundles. Air-side Reynolds numbers of 7.18×10^3 to 7.67×10^3 fell inside the range of validity of Equation (6). A clean-condition coefficient of 15.0 W m^{-2} K^{-1} referred to the total finned area corresponds to 320 W m^{-2} K^{-1} referred to the bare tube outside area, the form in which air-cooled exchanger design practice tabulates overall coefficients for hydrocarbon condensing duty [10].

These checks confirm that the model solves the equations it states and that its outputs are physically plausible. They do not validate it against the condition of this bundle. Validation in that sense requires a measured clean baseline or a documented deposit, and the plant holds neither for the observation period. The study therefore reports the ambient sensitivity of the indicator and reports no fouling state, a restriction carried through Section 3.7 and into the conclusions.

3. Results and Discussion

3.1. Ambient conditions over the observation period

Ambient temperature at the condenser fan inlet ranged from 18.63 to 29.56 °C over the 59-day record, averaging 22.48 °C with a standard deviation of 2.54 K across 471 observations. February averaged 22.31 °C and March 22.64 °C, a monthly difference of 0.33 K. The daily range averaged 6.57 K, and 21 of the 59 days fell below 4.5 K, coinciding with overcast and rain-affected conditions. Figure 4 shows the record and the daily range.

The within-day variation of 6.57 K is an order of magnitude larger than the between-month variation of 0.33 K, so an operator comparing this week's indicator against last

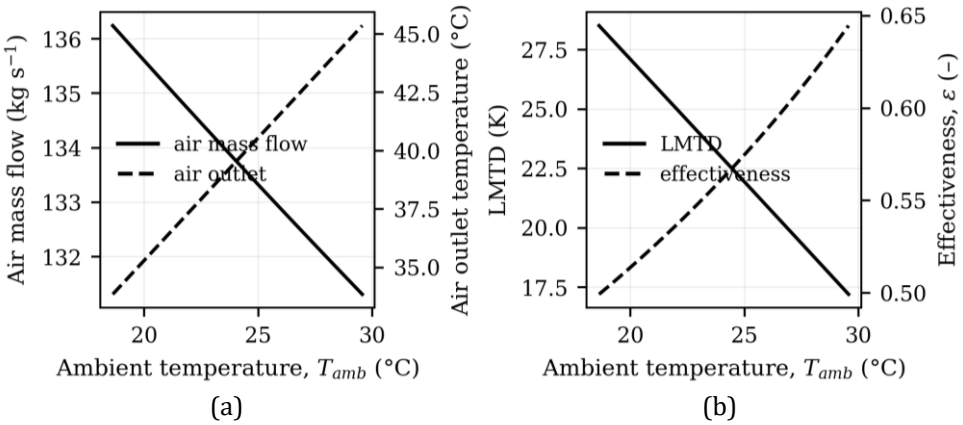


Figure 5. Base-case air-side response against ambient temperature: (a) cooling-air mass flow and the computed air outlet temperature, (b) log-mean temperature difference and exchanger effectiveness.

month's is comparing two points that differ far more in time of day than in season. Any indicator carrying an ambient sensitivity will therefore show a strong diurnal cycle superimposed on whatever slow trend deposition produces, and the diurnal component will dominate over the short windows on which maintenance decisions are usually taken.

3.2. Base-case thermal performance and resistance structure

Under the measured-air-flow route the cooling-air mass flow falls from 136.2 to 131.3 kg s^{-1} across the ambient range, a change of 3.6 %, arising solely from the reduction in air density as inlet temperature rises at constant volumetric flow. Computed air outlet temperature rises from 33.9 to 45.4 °C, tracking ambient almost one for one because the duty and the air mass flow are both nearly constant. Driving force consequently collapses, the log-mean temperature difference falling from 28.52 to 17.20 K, a loss of 39.7 %, while the exchanger effectiveness rises from 0.500 to 0.633. These quantities are shown in Figure 5.

The rise in effectiveness alongside the fall in driving force is not a contradiction but a consequence of which stream limits the exchanger. The working-fluid side carries the smaller heat-capacity rate, so effectiveness is referred to the working-fluid temperature change divided by the inlet temperature difference. Raising ambient temperature shrinks the inlet temperature difference while the working-fluid temperature change is fixed by the imposed states, so the ratio must rise. An operator reading effectiveness alone on a hot afternoon would conclude that the condenser had improved, which is the same artifact that this study traces in the fouling indicator.

The resistance network at the mean ambient condition divides as 58.7 % air side, 39.9 % tube side and 1.4 % wall, referred to the total finned outside area. Air side therefore carries the controlling resistance, with an air-side film coefficient of 47.4 W m^{-2} K^{-1} reduced by a weighted surface efficiency of 0.541 arising from a fin efficiency of 0.521. That the extended surface operates at under half efficiency is a direct consequence of the 15.8 mm fin height combined with a steel fin conductivity of 40 W m^{-1} K^{-1}. A steep temperature gradient develops along the fin, and roughly half the nominal 6,786 m^2 of surface is thermally inactive. The dominant resistance is also the one that is never measured, so any error or assumption on the air side propagates into the indicator at full weight.

3.3. Ambient response of the calculated fouling resistance

Each coefficient responds to ambient temperature in a different way, and it is that asymmetry that generates the apparent fouling signal. Figure 6 shows both.

The clean-condition coefficient is almost flat, falling 0.33 % from 15.051 to 15.002 W m^{-2} K^{-1} across the full 10.93 K range. This follows from Equation (10). Each of its three terms depends on ambient temperature only through air properties and the small density-driven change in mass flow, and the air-side Reynolds number falls only from 7.67×10^3 to 7.18×10^3. Its operating counterpart behaves quite differently, rising 74.5 % from 11.62 to 20.29 W m^{-2} K^{-1}. Equation (11) accounts for this. Duty is fixed and area is fixed, so U_d varies inversely with the product of F and the log-mean temperature difference, and that product falls by 42.7 % as the cold terminal is pushed upward. Under these conditions the operating coefficient is not measuring conductance at all. It is measuring the reciprocal of the driving force.

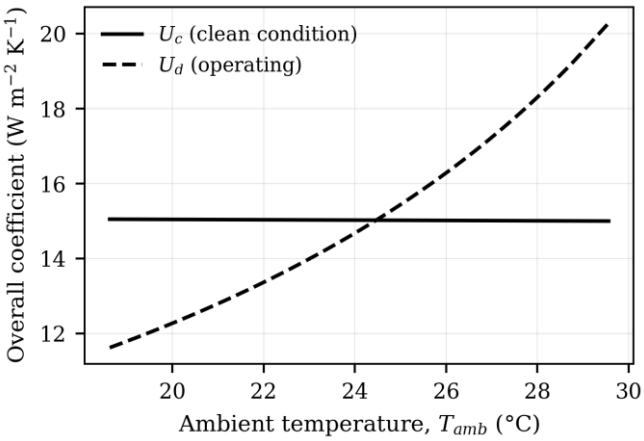


Figure 6. Clean-condition and operating overall heat-transfer coefficients against ambient temperature under the base-case route.

The calculated fouling resistance formed from these two coefficients therefore falls steeply with ambient temperature, from 1.96×10^{-2} to -1.74×10^{-2} m^2 K W^{-1}. Regression against ambient temperature gives a slope of -3.372×10^{-3} m^2 K W^{-1} per K with $R^2 = 0.99999$, which is effectively a deterministic relationship rather than a statistical association. Across the mean daily ambient range of 6.57 K the indicator swings by 2.22×10^{-2} m^2 K W^{-1}, which exceeds its own mean value of 6.66×10^{-3} m^2 K W^{-1} by a factor of 3.3. The indicator also crosses zero at 24.5 °C, near the middle of the observed range, so the same physically unchanged bundle reports positive fouling resistance in the early morning and negative fouling resistance in the afternoon.

The negative values that the indicator takes above 24.5 °C require interpretation, because a negative fouling resistance has no physical counterpart. A deposit can only add thermal resistance, so R_f is bounded below by zero and the negative sign belongs to the calculation rather than to the surface. Equation (12) forms R_d as the difference between the reciprocals of two coefficients obtained in different ways, and nothing in that construction prevents U_d from exceeding U_c. The operating coefficient rises with ambient temperature because the corrected log-mean temperature difference in the denominator of Equation (11) collapses faster than the duty falls, so U_d returns the reciprocal of the driving force. Its clean-condition counterpart stays almost fixed, depending on ambient temperature only through air properties. At 24.5 °C the operating coefficient therefore overtakes the clean-condition coefficient and the difference of reciprocals changes sign. A level error in the correlation-based U_c moves that

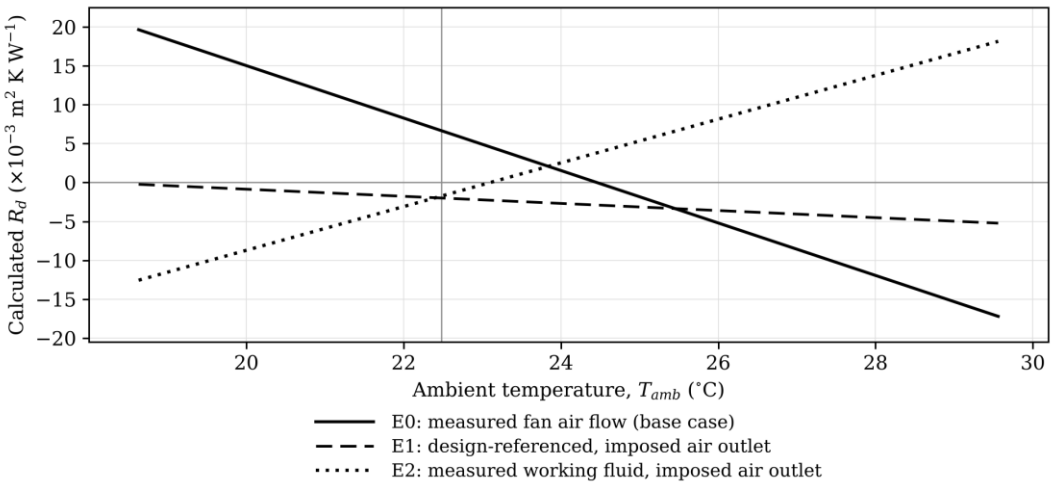


Figure 7. Calculated fouling resistance against ambient temperature under the three evaluation routes of Table 4. The routes differ only in which air-side quantity is treated as known. The vertical line marks the mean ambient temperature of the record.

crossing point as well, by the amount Section 3.4 quantifies, so the crossing temperature is not a property of the bundle either. A negative reading should be taken as evidence that the operating point has moved away from the conditions at which the clean reference was established, and never as evidence of a bundle in better than clean condition. The sign of R_d carries no information about surface condition unless the comparison is made within a matched ambient band.

Figure 7 shows how this behaviour depends on the air-side assumption, plotting the indicator along all three evaluation routes.

Route E1, the conventional design-referenced calculation, produces a slope of -4.57×10^{-4} m^2 K W^{-1} per K, a factor of 7.4 weaker than the base case, because imposing the air outlet temperature forces the air flow to rise with ambient temperature and so partially cancels the collapse in driving force. Route E2, which uses the recorded working-fluid states but keeps the imposed outlet temperature, reverses the sign entirely, giving $+2.81 \times 10^{-3}$ m^2 K W^{-1} per K. The three routes describe the same condenser over the same ambient range with the same correlations, and they disagree on whether apparent fouling increases or decreases with ambient temperature. Trend direction is therefore a property of the air-side assumption rather than of the equipment. This same asymmetry underlies the ACC performance sensitivities reported for thermal power plants under varying atmospheric conditions and under ambient wind, where the condenser response is likewise governed by the air-side terminal rather than by the exchanger surface [5], [6], [14].

This result extends rather than contradicts the monitoring literature. Patil et al. established that a fouling indicator inherits the dynamics of the mechanism holding the exchanger at its operating point, showing that a controller holding duty constant suppresses the fouling signal [12]. The present result is the corresponding statement for an exchanger with no such controller but with a moving heat sink. The indicator inherits the dynamics of the heat sink, and where the sink is not independently instrumented it inherits the dynamics of the assumption made in its place. Ambient sensitivities reported for air-cooled binary plants in the cycle-performance literature [1], [2], [4] are the same physics observed on the power output rather than on the condition indicator.

3.4. Sensitivity to the clean-condition model and parameter uncertainty

The four clean-condition treatments and the Monte Carlo perturbation separate the two uncertainties that the decomposition of Equation (13) distinguishes. Table 6 collects the results.

The four treatments move the mean level of the indicator from -6.57×10^{-2} to $+3.32 \times 10^{-2}$ m^2 K W^{-1}, a span of 9.9×10^{-2} that exceeds the magnitude of the base-case value and reverses its sign. Across all four, by contrast, the slope is identical to five significant figures. The reason is structural. Changing the clean-condition treatment shifts an additive offset in Equation (12) that is itself almost independent of ambient temperature, so the curve translates vertically without rotating. Monte Carlo perturbation carries the same message in the parameter domain. In 100 % of the 2,000 samples the slope is negative, with a 5th to 95th percentile band of only ±3.4 % about its central value, while the sign of the mean level is positive in 67.6 % of samples and its percentile band spans zero.

Fan flow was perturbed separately from the other parameters because it is the only air-side quantity in the model that rests on a single static measurement. Scaling the assumed fan volumetric flow between 0.80 and 1.20 of its measured value moved the mean level of the indicator from -4.0×10^{-3} to $+1.39 \times 10^{-2}$ m^2 K W^{-1}, a span of 1.8×10^{-2} m^2 K W^{-1} that again exceeds the base-case value, while the ambient slope changed by less than 0.2 %. Replacing the constant-volumetric-flow treatment with constant mass flow, which is the opposite limit of fan behaviour over a varying inlet density, changed the slope from -3.372×10^{-3} to -3.23×10^{-3} m^2 K W^{-1} per K, a weakening of 4.3 %, and left the mean level unchanged. Variation in

Table 6. Sensitivity of the calculated fouling resistance to the clean-condition treatment and to parameter perturbation.

Case	R_d at Mean Ambient (m^2 K W^{-1})	Slope (m^2 K W^{-1} per K)
Duty-weighted tube side (base case)	$+6.66 \times 10^{-3}$	-3.3722×10^{-3}
Condensation coefficient only	$+1.92 \times 10^{-2}$	-3.3722×10^{-3}
Single-phase liquid only	-6.57×10^{-2}	-3.3722×10^{-3}
Zero tube-side resistance	$+3.32 \times 10^{-2}$	-3.3722×10^{-3}
Monte Carlo, 5th to 95th percentile	-1.23×10^{-2} to $+1.77 \times 10^{-2}$	-3.49×10^{-3} to -3.26×10^{-3}

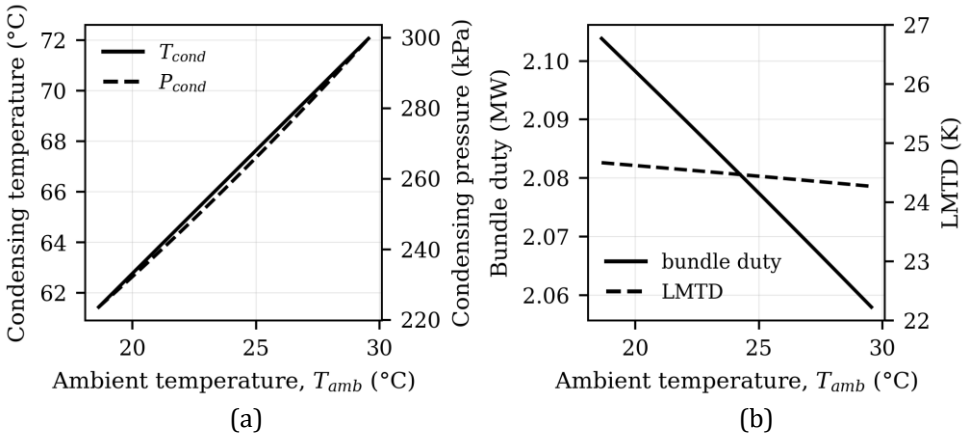


Figure 8. Coupled closed-loop response at fixed fan volumetric flow: (a) condensing temperature and condensing pressure, (b) bundle duty and log-mean temperature difference.

real fan performance therefore enters the indicator in the same way as the clean-condition treatment, by setting the level rather than the ambient dependence, and bounding the fan between its two physical limits changes the reported slope by less than 5 %.

The two uncertainties are not of the same kind and cannot be treated with the same remedy. Available information does not determine the magnitude of the calculated fouling resistance, even as to its sign, and improving the clean-condition correlation would reduce that offset. The ambient dependence is determined, and no improvement to the correlation touches it. In the language of Equation (13), a better correlation addresses R_{model} while leaving R_{amb} unchanged. Studies of fouling estimation in heat exchanger networks reach the same conclusion, that an estimated resistance must be read against the property and operating assumptions used to produce it [13].

3.5. Coupled cycle response

The coupled model establishes how far the real operating point moves over the same ambient range, and therefore how much of the fixed-duty idealisation is a simplification rather than an error. Figure 8 shows the results.

The condensing temperature rises from 61.4 to 72.1 °C, a sensitivity of 0.973 K per K of ambient, and the condensing pressure rises from 223.6 to 299.7 kPa at 6.86 kPa per K. Exchanger conductance and air flow are both nearly fixed, so the only way for the bundle to reject a nearly constant duty against a warmer sink is to raise its own temperature until the driving force is restored. This is why the log-mean temperature difference stays almost flat at 24.7 to 24.3 K in the coupled solution, while it collapsed by 39.7 % in the fixed-condensing-temperature analysis of Section 3.2. Bundle duty falls only 0.200 % per K, confirming that the near-constant-duty treatment is a reasonable idealisation for the indicator analysis even though the condensing conditions are not.

The turbine consequence follows from the pressure. Taking the first-order isentropic sensitivity at the recorded exhaust specific volume, the 6.86 kPa per K rise in back pressure corresponds to a power penalty of approximately 117 kW per K per unit. For external corroboration, Kahraman et al. report a 6.8 MW loss over a 30 K ambient rise for a 21 MW air-cooled binary plant, equivalent to 227 kW per K on a unit roughly twice the size of the one modelled here [1]. Agreement in order of magnitude supports the coupled formulation. It is not a validation, and is not presented as one. The present study has no measured condensing-pressure record against which to test the predicted 6.86 kPa per K.

3.6. Implications for condition monitoring

These results place a concrete limit on how the overall-coefficient method can be used on an ACC of this type. An indicator whose diurnal swing of 2.22×10^{-2} m^2 K W^{-1} exceeds its own mean value by a factor of 3.3 cannot resolve a slow deposition trend unless ambient temperature is controlled for, and an indicator that changes sign at 24.5 °C cannot be compared against a fixed threshold at all. Three measures follow directly from the mechanism identified, and none requires major modification to the existing monitoring system.

Table 7. Conditions under which each evaluation route is appropriate for condition monitoring.

Route	Appropriate When	Output Supports	Output Does Not Support
E0 (base case)	Fan air flow measured, or fan speed and fan curve logged	Trending within matched ambient bands of ±1 K or narrower; step change across a cleaning	Comparison against a fixed threshold; readings taken outside a matched band
E1	Only a design data sheet available	Coarse check that the unit is near its design point	Trending of surface condition, since the reference is design duty and design T_{cond}
E2	Working-fluid states recorded, no air-side measurement	Nothing on its own, because the air-side duty equals the working-fluid duty by construction	Direction of a fouling trend, since the imposed outlet temperature reverses the slope to $+2.81 \times 10^{-3}$ m^2 K W^{-1} per K

First, comparisons should be made within matched ambient bands rather than against a fixed reference. At the measured slope, a ±1 K band admits a spread of 6.7×10^{-3} m^2 K W^{-1} from ambient variation alone, and a ±0.2 K band reduces this to 1.3×10^{-3}. Since the plant record carries eight observations per day across a 6.57 K daily range, narrow bands are populated within a few weeks without any new instrumentation, simply by filtering the existing history. Second, the clean baseline should be plant-specific and expressed as a function of ambient temperature rather than as a single number, because Table 6 shows the level to be undetermined while the ambient response is determined. A baseline fitted to the plant's own early-life operating data removes the offset that no correlation can supply. Third, independent indicators should be read alongside R_d. Air-side pressure drop and fan motor current respond to the flow blockage that accompanies fin-side deposition and are largely insensitive to the driving-force collapse that dominates the thermal indicator, so they fail differently and provide genuine corroboration rather than a second view of the same artifact. This is the same reasoning that leads process-side studies to combine thermal and hydraulic loads rather than relying on a thermal indicator alone [11], [12], and to schedule cleaning against an explicit operating-constraint model rather than against a raw trend [15].

The three evaluation routes are not interchangeable, and the choice among them should follow the instrumentation actually fitted rather than convention. Table 7 states the condition under which each route is appropriate for condition monitoring and what its output can and cannot support.

For maintenance scheduling, the consequence is that a rising R_d trend observed over a cooling season should not trigger a cleaning decision on its own. At this plant a seasonal ambient shift of 0.33 K between months generates an apparent change of 1.1×10^{-3} m^2 K W^{-1}, which is of the same order as the deposition signal accumulated over comparable periods in published finned-tube fouling studies [7], [8]. An unnecessary bundle cleaning carries both the direct cost of the work and the availability cost of the outage, while a missed genuine fouling trend carries a continuous generation penalty through elevated condensing pressure at the rate established in Section 3.5. Ambient correction is therefore not a refinement of the monitoring method but a precondition for using it to make either decision.

3.7. Limitations

Four limitations bound these results. The air side rests on a single static velocity measurement rather than a logged record, so the base-case air flow is constant by assumption and any real variation in fan performance, blade pitch or air maldistribution lies outside the model. A ±15 % velocity perturbation in the Monte Carlo analysis and the fan-flow scan of Section 3.4 test sensitivity to this but do not substitute for measurement. The fan velocity is referred to the fan area given on the data sheet, and reading it instead as a velocity at the bundle face or between the fins changes the base-case level of R_d by roughly a factor of two, although it leaves the slope essentially unchanged. No validation against a documented cleaning event or a direct deposit measurement was available, which is the central limitation of the study. It establishes the ambient sensitivity of the indicator and it establishes nothing about the fouling state of this bundle, and no result reported here should be read as confirming that the condenser is fouled or that it is clean. An observation period of 59 days covers a 10.93 K ambient range but not a full annual cycle, so the findings describe this plant over 1 February

to 31 March 2026 and are not generalised to a seasonal cycle or to other condensers without re-evaluation.

Environmental variables other than dry-bulb temperature lay outside the model and would add further movement to the indicator. Humidity changes the air density, and at the pressure and temperatures of this record a shift from dry to saturated air lowers it by 0.9 % at 20 °C and 1.6 % at 30 °C, which enters the air mass flow in the same way as the 3.6 % density change already resolved. Wind alters the flow distribution at the fan inlet and can drive heated plume air back into the bundle, which raises the effective inlet temperature above the measured ambient value and so displaces the indicator along the slope reported here with no change in the weather station reading. Rain wets the fin surface and adds an evaporative component to the air-side heat transfer that the dry-surface correlation of Equation (6) does not represent, and the 21 days of the record with a daily range below 4.5 K coincided with overcast and rain-affected conditions. Air-flow maldistribution across the bundle face changes the local driving force without changing the measured fan velocity. None of these effects was instrumented at this plant, and each would act on the level or the slope of the indicator in addition to the dry-bulb dependence quantified here.

The analysis is also not an acceptance test. ASME PTC 30 prescribes the instrumentation, steady-state criteria and uncertainty accounting required for a code-grade performance test of air-cooled heat exchangers, including measured air flow and inlet and outlet air temperatures, none of which the routine plant record supplies. This work is a condition-monitoring analysis of operating data and is positioned as complementary to, not a substitute for, a PTC 30 test. Where a plant requires a defensible statement of fouling condition rather than a trend, a code-grade test remains the appropriate instrument, and the instrumentation it specifies is precisely what would close the gap identified here.

Logging fan motor current and installing air outlet temperature measurement on one bundle would convert the imposed boundary of routes E1 and E2 into a measured one, allowing the three routes to be tested against each other on real data. Recording condensing pressure alongside ambient temperature over a full season would test the predicted 6.86 kPa per K directly. A documented cleaning event, with the indicator tracked before and after under matched ambient conditions, would establish the deposition signal against which the ambient artifact must be separated.

4. Conclusions

Ambient-temperature variation alone generated a change in the calculated fouling resistance of the air-cooled condenser that exceeded the magnitude of the indicator itself. Over the measured ambient range of 18.63 to 29.56 °C, with physical fouling held constant by construction, the indicator fell at 3.372×10^{-3} m^2 K W^{-1} per K and swung by 2.22×10^{-2} m^2 K W^{-1} across an average day against a mean value of 6.66×10^{-3} m^2 K W^{-1}. It changed sign at 24.5 °C. The negative values carry no physical meaning, because a deposit cannot reduce thermal resistance, and they mark the ambient temperature at which the operating coefficient overtakes the correlation-based clean-condition coefficient. The mechanism was the asymmetric response of the two coefficients from which the indicator is formed. Across the range the clean-condition coefficient varied by 0.33 % while the operating coefficient rose 74.5 % as the corrected log-mean temperature difference collapsed. The indicator reported the driving force rather than the conductance. Two classes of result should be distinguished. The ambient record, the working-fluid states, the bundle duty, the fan velocity and the bundle geometry were measured at the plant. Heat-transfer coefficients, the three evaluation routes, the clean-condition treatments and the coupled cycle response were computed from correlations and are model outputs. A predicted rise in condensing pressure of 6.86 kPa per K and the associated turbine penalty of approximately 117 kW per K per unit belong to the second class and were not tested against a measured condensing-pressure record.

The reported direction of the trend followed the air-side assumption rather than the equipment. Fixing air flow from the measured fan data gave a negative slope, the conventional design-referenced treatment weakened it by a factor of 7.4, and imposing the air outlet temperature with recorded working-fluid states reversed its sign. Four clean-condition treatments moved the level of the indicator across zero while leaving the slope unchanged, an error in the assumed fan flow did the same, and the slope remained negative in 100 % of 2,000 Monte Carlo samples under both independent and correlated sampling. Available information leaves the magnitude of the indicator undetermined. Its ambient dependence is determined and is inherent to the formulation.

For maintenance decisions the consequence is that a rising or falling trend in the calculated fouling resistance of an ACC is not by itself evidence that cleaning is needed or that the bundle is clean. The indicator should be compared only within matched ambient bands, where a ±1 K band limits the ambient-generated spread to 6.7×10^{-3} m^2 K W^{-1} and a ±0.2 K band to 1.3×10^{-3}, referenced to a plant-specific clean baseline expressed as a function of ambient temperature, and read alongside independent indicators such as air-side pressure drop or fan motor current. All three are achievable at this plant by filtering the existing three-hourly record and reading instruments already fitted.

These results establish the ambient sensitivity of the indicator for one binary geothermal ACC over a 59-day period and do not establish the fouling state of the bundle examined, which would require a measured clean baseline or a direct deposit measurement that the plant does not hold. That record spans 10.93 K of ambient variation but not a full annual cycle, so the slope reported here is not extrapolated to seasonal extremes or transferred to other condensers. Logging fan motor current and instrumenting air outlet temperature on one bundle, recording condensing pressure against ambient temperature over a full year, and tracking the indicator across a documented cleaning under matched ambient conditions would close these gaps.

Acknowledgements

The authors thank the Master of Energy Program, School of Postgraduate Studies, Universitas Diponegoro, Semarang, Indonesia, for the academic supervision and institutional support provided throughout this work. The authors also thank the management and technical personnel of the investigated geothermal power plant for granting access to the operating data and equipment documentation on which the analysis is based. Neither party is listed as an author of this manuscript.

Declaration of Generative AI and AI-Assisted Technologies in the Writing Process

The authors used Grammarly (Grammarly Inc.) during the preparation of this manuscript to assist with language editing of the English text, specifically grammar, spelling, punctuation and sentence clarity. All suggestions produced by the tool were critically reviewed, revised and validated by the authors. The authors take full responsibility for the scientific accuracy, originality and integrity of the manuscript, in accordance with the guidelines of the Committee on Publication Ethics (COPE).

References

[1] M. Kahraman, A. B. Olcay, and E. Sorgüven, "Thermodynamic and thermoeconomic analysis of a 21 MW binary type air-cooled geothermal power plant and determination of the effect of ambient temperature variation on the plant performance," *Energy Convers. Manage.*, vol. 192, pp. 308–320, 2019, doi: 10.1016/j.enconman.2019.04.036.

[2] M. Astolfi, M. C. Romano, P. Bombarda, and E. Macchi, "Binary ORC (organic Rankine cycles) power plants for the exploitation of medium–low temperature geothermal sources—Part A: Thermodynamic optimization," *Energy*, vol. 66, pp. 423–434, 2014, doi: 10.1016/j.energy.2013.11.056.

[3] A. S. Zavorin, S. V. Lavrinenko, S. Tsibulskiy, S. A. Yankovsky, P. Berezny, and N. S. Yankovskaya, "Numerical studies of an air-cooled condenser as part of the thermal diagram of a binary geothermal power plant," *Therm. Sci. Eng. Prog.*, vol. 66, Art. no. 103969, 2025, doi: 10.1016/j.tsep.2025.103969.

[4] O. V. Güler, "Optimal photovoltaic integration for offsetting temperature-dependent auxiliary electricity demand in an air-cooled geothermal power plant," *Energies*, vol. 19, no. 20, Art. no. 4768, 2026, doi: 10.3390/en19204768.

[5] J. B. Škundrić, P. M. Živković, M. M. Tica, M. A. Tomić, and C. P. Barz, "Investigation of air-cooled condenser's operating parameters in modern thermal power plant," *Therm. Sci.*, vol. 27, no. 3B, pp. 2477–2487, 2023, doi: 10.2298/TSCI220806203S.

[6] X. Zhu, T. Yu, J. Zhan, and Y. Zhou, "Investigation of the performance of cold-end system in direct air-cooled power units under the influence of ambient winds," *Therm. Sci.*, vol. 28, no. 3B, pp. 2433–2446, 2024, doi: 10.2298/TSCI230609046Z.

[7] H. V. Inamdar, E. A. Groll, J. A. Weibel, and S. V. Garimella, "Air-side fouling of finned heat exchangers: Part 1, review and proposed test protocol," *Int. J. Refrig.*, vol. 151, pp. 77–86, 2023, doi: 10.1016/j.ijrefrig.2023.02.017.

[8] H. V. Inamdar, E. A. Groll, J. A. Weibel, and S. V. Garimella, "Air-side fouling of finned heat exchangers: Part 2, experimental investigation and assessment of test protocol," *Int. J. Refrig.*, vol. 151, pp. 63–76, 2023, doi: 10.1016/j.ijrefrig.2023.03.016.

[9] L. Morozyuk, V. Sokolovska-Yefymenko, A. Moshkatiuk, V. Ierin, and A. Basov, "Experimental study and analysis of an air-cooled condenser with the fouling on the heat exchange surface for small-scale commercial refrigeration systems," *Int. J. Air-Conditioning Refrig.*, vol. 31, Art. no. 18, 2023, doi: 10.1007/s44189-023-00034-8.

[10] R. W. Serth and T. G. Lestina, *Process Heat Transfer: Principles, Applications and Rules of Thumb*, 2nd ed. Oxford, U.K.: Academic Press, 2014, doi: 10.1016/C2011-0-07242-3.

[11] X. Mei, H. Kiyomoto, S. Kato, and Y. Kansha, "Data-driven soft sensor for crude oil fouling monitoring in heat exchanger networks," *IEEE Sens. J.*, vol. 23, no. 21, pp. 26336–26346, 2023, doi: 10.1109/JSEN.2023.3317936.

[12] P. Patil, B. Srinivasan, and R. Srinivasan, "Monitoring fouling in heat exchangers under temperature control based on excess thermal and hydraulic loads," *Chem. Eng. Res. Des.*, vol. 181, pp. 41–54, 2022, doi: 10.1016/j.cherd.2022.02.032.

[13] J. P. V. de Cesaro, M. A. S. S. Ravagnani, and C. B. B. Costa, "Variable properties in fouling estimation in heat exchanger networks with fouling," *Heat Transfer Eng.*, early access, Jul. 12, 2026, doi: 10.1080/01457632.2026.2697387.
[14] F. S. Marincowitz, M. T. F. Owen, and J. Muiyser, "Multi-objective optimisation for wind resistant air-cooled condenser operation," *Appl. Therm. Eng.*, vol. 218, Art. no. 119382, 2023, doi: 10.1016/j.applthermaleng.2022.119382.
[15] S. B. Dekebo, G.-T. Oh, and M.-W. Lee, "Cleaning schedule optimization of heat exchanger network using moving window decision-making algorithm," *Appl. Sci.*, vol. 13, no. 1, Art. no. 604, 2023, doi: 10.3390/app13010604.
[16] I. H. Bell, J. Wronski, S. Quoilin, and V. Lemort, "Pure and pseudo-pure fluid thermophysical property evaluation and the open-source thermophysical property library CoolProp," *Ind. Eng. Chem. Res.*, vol. 53, no. 6, pp. 2498–2508, 2014, doi: 10.1021/ie4033999.
[17] M. M. Shah, "A general correlation for heat transfer during film condensation inside pipes," *Int. J. Heat Mass Transfer*, vol. 22, no. 4, pp. 547–556, 1979, doi: 10.1016/0017-9310(79)90058-9.
[18] W. M. Kays and A. L. London, *Compact Heat Exchangers*, 3rd ed. New York, NY, USA: McGraw-Hill, 1984.
[19] R. K. Shah and D. P. Sekulić, *Fundamentals of Heat Exchanger Design*. Hoboken, NJ, USA: John Wiley & Sons, 2003, doi: 10.1002/9780470172605.
[20] K. Shaikh *et al.*, "Improvement of heat transfer and fouling retardation performance of heat exchanger using green functionalized graphene nanoplatelets additives," *J. Taiwan Inst. Chem. Eng.*, vol. 153, Art. no. 105227, 2023, doi: 10.1016/j.jtice.2023.105227.
[21] K. Shaikh *et al.*, "Retardation of CaCO3 fouling on heat exchanger surface using water-based cloves-functionalized multiwall carbon nanotubes (C-MWCNT) nanofluids," *J. Therm. Anal. Calorim.*, vol. 148, no. 22, pp. 12937–12946, 2023, doi: 10.1007/s10973-023-12551-0.
[22] K. Shaikh *et al.*, "Performance evaluation of green synthesized graphene nanoplatelets/multiwall carbon nanotubes hybrid nanofluids for the retardation of mineral fouling and its environmental benefits," *Carbon*, vol. 238, Art. no. 120243, 2025, doi: 10.1016/j.carbon.2025.120243.
[23] S. Abdullah, K. Shaikh, S. N. Kazi, and M. N. M. Zubir, "Inhibition of CaCO3 scaling on heat exchanger surface with green functionalized graphene nanoplatelets (GGNP) coating," *Therm. Sci. Eng. Prog.*, vol. 65, Art. no. 103962, 2025, doi: 10.1016/j.tsep.2025.103962.
[24] K. Shaikh *et al.*, "Comparative study on inhibition of mineral scaling on heat exchanger surface with green functionalized graphene nanoplatelets, multiwall carbon nanotubes, and their hybrid," *Chem. Eng. Res. Des.*, vol. 222, pp. 313–324, 2025, doi: 10.1016/j.cherd.2025.09.012.
[25] A. Ahmed, K. Shaikh, S. N. Kazi, M. N. M. Zubir, R. Nawaz, and S. U. Hasnain, "A critical review on mitigation of crystallization fouling in heat exchangers through surface modification," *Surf. Interfaces*, vol. 94, Art. no. 109493, 2026, doi: 10.1016/j.surfin.2026.109493.
[26] X. Xie, Y. Chen, L. Dai, and L. Xu, "Modeling and experimental study of air-cooled finned-tube condenser using coupled distribution parameter method and air-side temperature distribution," *Appl. Therm. Eng.*, vol. 249, Art. no. 123411, 2024, doi: 10.1016/j.applthermaleng.2024.123411.